Computation of correlation-induced atomic displacements and structural transformations in paramagnetic KCuF$_3$ and LaMnO$_3$

I. Leonov,[1] Dm. Korotin,[2] N. Binggeli,[3] V. I. Anisimov,[2] and D. Vollhardt[1]

^{1}*Theoretical Physics III, Center for Electronic Correlations and Magnetism,*

Institute of Physics, University of Augsburg, Augsburg 86135, Germany

^{2}*Institute of Metal Physics, S. Kovalevskoy St. 18,*

620219 Yekaterinburg GSP-170, Russia

^{3}*Abdus Salam International Center for Theoretical Physics and*

INFM-CNR Democritos National Simulation Center, Trieste 34014, Italy

Abstract

We present a computational scheme for *ab initio* total-energy calculations of materials with strongly interacting electrons using a plane-wave basis set. It combines *ab initio* band structure and dynamical mean-field theory and is implemented in terms of plane-wave pseudopotentials. The present approach allows us to investigate complex materials with strongly interacting electrons and is able to treat atomic displacements, and hence structural transformations, caused by electronic correlations. Here it is employed to investigate two prototypical Jahn-Teller materials, KCuF$_3$ and LaMnO$_3$, in their paramagnetic phases. The computed equilibrium Jahn-Teller distortion and antiferro-orbital order agree well with experiment, and the structural optimization performed for paramagnetic KCuF$_3$ yields the correct lattice constant, equilibrium Jahn-Teller distortion and tetragonal compression of the unit cell. Most importantly, the present approach is able to determine correlation-induced structural transformations, equilibrium atomic positions and lattice structure in both strongly and weakly correlated solids in their *paramagnetic* phases as well as in phases with long-range magnetic order.

PACS numbers: 71.10.-w, 71.15.Ap, 71.27.+a

I. INTRODUCTION

The theoretical understanding of complex materials with strongly interacting electrons is one of the most challenging areas of current research in condensed matter physics. Experimental studies of such materials have often revealed rich phase diagrams originating from the interplay between electronic and lattice degrees of freedom.[1] This makes these compounds particularly interesting in view of possible technological applications. Namely, the great sensitivity of many correlated electron materials with respect to changes of external parameters such as temperature, pressure, magnetic and/or electric field, doping, etc., can be employed to construct materials with useful functionalities.[1]

The electronic properties of materials can be computed from first principles by density functional theory in the local density approximation (LDA),[2] the generalized gradient approximation (GGA),[3,4] or using the so-called LDA+U method.[5,6] Applications of these approaches accurately describe the phase diagrams of many simple elements and semiconductors, and of some insulators. Moreover, they often allow to make correct qualitative predictions of the magnetic, orbital, and crystal structures of solids, where the equilibrium (thermodynamic) structures are determined by simultaneous optimization of the electron and lattice systems.[7,8,9,10,11,12] However, these methods usually fail to describe the correct electronic and structural properties of electronically correlated *paramagnetic* materials. Hence the computation of electronic, magnetic, and structural properties of strongly correlated paramagnetic materials remains a great challenge.

Here the recently developed combination of conventional band structure theory and dynamical mean-field theory,[13] the so-called LDA+DMFT computational scheme,[14] has become a powerful tool for the investigation of strongly correlated compounds in both their paramagnetic and magnetically ordered states. In particular, it provides important insights into the spectral and magnetic properties of correlated electron materials,[15,16] especially in the vicinity of a Mott metal-insulator transition as encountered in transition metal oxides.[1] Up to now implementations of the LDA+DMFT approach utilized linearized and higher-order muffin-tin orbital [L(N)MTO] techniques[17] and focused on the investigation of electronic correlation effects for a given lattice structure. However, the mutual interaction between electrons and ions, i.e., the influence of the electrons on the lattice structure, is then completely neglected. LDA+DMFT computations of the volume collapse in paramagnetic Ce[18,19] and Pu[20] and of

the collapse of the magnetic moment in MnO[21] did include the lattice, but only calculated the total energy of the correlated material as a function of the unit cell volume.[22] In the case of more subtle structural transformations, e.g., involving the cooperative Jahn-Teller (JT) effect,[23,24] the L(N)MTO technique is not suitable since it cannot reliably determine atomic positions. This is due to the atomic-sphere approximation within the L(N)MTO scheme, where a spherical potential inside the atomic sphere is employed. Thereby multipole contributions to the electrostatic energy due to the distorted charge density distribution around the atom are ignored. Instead, the recently proposed implementation of the LDA+DMFT approach, which employs plane-wave pseudopotentials[25,26,27,28,29] and thus avoids the atomic sphere approximation, does not neglect such contributions. Thereby it becomes possible to describe the effect of the distortion on the electrostatic energy.[25]

In this paper, we present a detailed formulation of the LDA+DMFT scheme implemented with plane-wave pseudopotentials reported earlier.[25,26] This scheme allows us to compute structural transformations (e.g., structural phase stability and structure optimization) caused by electronic correlations. Most importantly, it is able to determine correlation-induced structural transformations in both paramagnetic solids and long-range ordered solids. Therefore, the present computational scheme overcomes the limitations of standard band-structure approaches and opens the way for fully microscopic investigations of the structural properties of strongly correlated electron materials.

We apply this method to study orbital order and the cooperative JT distortion in two prototypical JT materials, $KCuF_3$ and $LaMnO_3$, and compute the electronic, structural, and orbital properties in their room-temperature paramagnetic phase. At room temperature, both compounds have a distorted perovskite structure with a strong cooperative JT distortion. Considering this structural complexity, $KCuF_3$ has a relatively high (tetragonal) symmetry,[30] where only the cooperative JT distortion of the CuF_6 octahedra is responsible for the deviation from the cubic perovskite symmetry. $LaMnO_3$ instead crystallizes in a more complex (orthorhombic) structure in which MnO_6 octahedra are simultaneously JT distorted and tilted with respect to the ideal cubic perovskite structure.[31,32,33] The JT distortion persists up to the melting temperature ~ 1000 K in $KCuF_3$. By contrast, in $LaMnO_3$ it persists only up to $T_{JT} \sim 750$ K, the temperature at which the JT distortion vanishes and where $LaMnO_3$ undergoes a structural phase transition with a volume collapse to a nearly cubic structure without JT distortion and orbital order.[32,33] Concerning the electronic con-

figuration, $KCuF_3$ nominally has a Cu^{2+} $3d^9$ structure, i.e., a single hole in the $3d$ shell. By contrast, due to Hund's rule coupling $LaMnO_3$ has a single $e_{g\uparrow}$ electron bound to the fully spin-polarized three $t_{2g\uparrow}$ electrons in a high spin $3d^4$ ($t_{2g\uparrow}^3 e_{g\uparrow}^1$) electronic configuration. To properly describe this correlated state, a different treatment compared to $KCuF_3$ is required, which takes into account the effective on-site spin interaction between t_{2g} and e_g electrons.[34,35] At low temperatures, both systems display A-type long-range antiferromagnetic order, consistent with the Goodenough-Kanamori-Anderson rules for a superexchange interaction with antiferro-orbital order. In both compounds the Néel temperature ($T_N \sim 38$ K in $KCuF_3$ and $T_N \sim 140$ K in $LaMnO_3$) is remarkably lower than T_{JT}.

In this paper we will show that our approach can explain the orbital order, cooperative JT distortion, and related structural properties in both materials, in spite of their chemical, structural, and electronic differences. The scheme is robust and makes it possible to address, on the same footing, electronic, magnetic, and structural properties of strongly correlated materials.

The paper is organized as follows. In Section II we present computational details needed to reproduce the results of our calculations. The crystal structures, magnetic properties, and results of electronic structure calculations of paramagnetic $KCuF_3$ and $LaMnO_3$ are presented in Sections III and IV, respectively. Finally, the results are summarized in Section V.

II. COMPUTATIONAL DETAILS

In order to compute the electronic structure of correlated electron materials, we have implemented DMFT within a realistic electronic structure approach, which is formulated in terms of plane-wave pseudopotentials.[25,26] Following the paper of Anisimov et $al.$[36] and Trimarchi et $al.$,[26] this can be achieved by applying a projection onto atomic-centered symmetry-constrained Wannier orbitals,[37] which gives an effective low-energy Hamiltonian $\hat{H}_{DFT}$ for the partially filled correlated orbitals (e.g., $3d$ orbitals of transition metal ion).

The Hamiltonian $\hat{H}_{DFT}$ provides a realistic description of the material's single-electron band structure. It is supplemented by on-site Coulomb interactions for the correlated or-

bitals, resulting in a many-body Hamiltonian of the form:

$$\hat{H} = \hat{H}_{DFT} + U \sum_{im} \hat{n}_{im\uparrow} \hat{n}_{im\downarrow}$$
$$+ \sum_{im \neq m'\sigma\sigma'} (V - \delta_{\sigma\sigma'} J) \hat{n}_{im\sigma} \hat{n}_{im'\sigma'} - \hat{H}_{DC}. \tag{1}$$

Here the second and third terms on the right-hand side describe the local Coulomb inter-action between electrons in the same and in different correlated orbitals, respectively, with $V = U - 2J$, and $\hat{H}_{DC}$ is a double counting correction which accounts for the electronic in-teractions already described by DFT (see below). The Coulomb repulsion U and Hund's rule exchange J can be evaluated using a constrained DFT scheme within a Wannier-functions formalism, making the Hamiltonian (1) free of adjustable parameters.[27]

The many-body Hamiltonian (1) is then solved by dynamical mean-field theory (DMFT)[13] with the effective impurity model treated, e.g., by the numerically exact Hirsch-Fye quantum Monte-Carlo method.[38] Finally, applying a maximum entropy treatment of Monte-Carlo data, one obtains the real-frequency spectral functions, which can be further compared to physically observable spectra.

The total energy is another important quantity which can be evaluated from DFT+DMFT calculation using the following expression[19,25]

$$E = E_{DFT}[\rho] + \langle \hat{H}_{DFT} \rangle - \sum_{m,k} \epsilon_{m,k}^{DFT} + \langle \hat{H}_U \rangle - E_{DC}. \tag{2}$$

Here $E_{DFT}[\rho]$ is the total energy obtained by DFT. The third term on the right-hand side of Eq. (2) is the sum of the DFT valence-state eigenvalues which is evaluated as the thermal average of the DFT Hamiltonian with the non-interacting DFT Green's function $G_{\mathbf{k}}^{DFT}(i\omega_n)$:

$$\sum_{m,k} \epsilon_{m,k}^{DFT} = T \sum_{i\omega_n,\mathbf{k}} Tr[H_{DFT}(\mathbf{k}) G_{\mathbf{k}}^{DFT}(i\omega_n)] e^{i\omega_n 0^+}. \tag{3}$$

In this expression, we have assumed that the DFT total energy has only a weak temper-ature dependence via the Fermi distribution function, i.e., one neglects the temperature dependence of the exchange-correlation potential. $\langle \hat{H}_{DFT} \rangle$ is evaluated similarly but with the full Green's function including the self-energy. To calculate these two contributions, the summation is performed over the Matsubara frequencies $i\omega_n$ (typically with $n_{max} = 10^3$), taking into account an analytically evaluated asymptotic correction (see below). Thus, for

$\langle \hat{H}_{DFT} \rangle$ one has

$$\langle \hat{H}_{DFT} \rangle = T \sum_{i\omega_n, \mathbf{k}} Tr[H_{DFT}(\mathbf{k})G_{\mathbf{k}}(i\omega_n)]e^{i\omega_n 0^+}$$

$$= T \sum_{i\omega_n, \mathbf{k}}^{\pm i\omega_{n_{max}}} Tr\{H_{DFT}(\mathbf{k})[G_{\mathbf{k}}(i\omega_n) - \frac{m_1^{\mathbf{k}}}{(i\omega_n)^2}]\}$$

$$+ \frac{1}{2} \sum_{\mathbf{k}} Tr[H_{DFT}(\mathbf{k})] - \frac{1}{4T} \sum_{\mathbf{k}} Tr[H_{DFT}(\mathbf{k})m_1^{\mathbf{k}}] \qquad (4)$$

where the first moment $m_1^{\mathbf{k}}$ is computed as $m_1^{\mathbf{k}} = H_{DFT}(\mathbf{k}) + \Sigma(i\infty) - \mu$; the asymptotic part of the self-energy $\Sigma(i\infty)$ is calculated as the average of $\Sigma(i\omega_n)$ over the last several $i\omega_n$ points. The interaction energy $\langle \hat{H}_U \rangle$ is computed from the double occupancy matrix. The double-counting correction E_{DC} is evaluated as the average Coulomb repulsion between the N_d correlated electrons in the Wannier orbitals. In the case of a paramagnet it corresponds to $E_{DC} = \frac{1}{2}UN_d(N_d - 1) - \frac{1}{4}JN_d(N_d - 2)$. Since the Hamiltonian involves only correlated orbitals the number of Wannier electrons N_d is conserved. Therefore, the double-counting correction amounts to an irrelevant shift of the total energy.

Within this approach, we can determine correlation-induced structural transformations, as well as the corresponding change of the atomic coordinates and of the unit cell shape. The result can be further used to explain the experimentally observed structural data and to predict structural properties of real correlated materials. In Sections III and IV we will apply this method to determine the orbital order and the cooperative JT distortion in the paramagnetic phase of two prototypical JT systems $KCuF_3$ and $LaMnO_3$.

III. APPLICATION TO KCuF$_3$

A. Crystal structure and magnetic properties

$KCuF_3$ is the prototype of a material with a cooperative Jahn-Teller (JT) distortion, orbital order, and low-dimensional magnetism.[24,39] At room temperature it crystallizes in a pseudocubic perovskite crystal structure[30] which is related to the crystal structure of high-T_c superconductors and colossal magnetoresistance manganites and, particularly, to their parent compound, $LaMnO_3$. Due to the particular orbital order in $KCuF_3$ it is one of the rare examples of an ideal one-dimensional antiferromagnetic Heisenberg system.[24] Thus, the

copper ions have an octahedral fluorine surrounding and are nominally in a Cu^{2+} ($3d^9$) electronic configuration with a single hole in the e_g states. This gives rise to a strong JT instability that lifts the cubic degeneracy at Cu e_g states due to a cooperative JT distortion.[24] The latter is characterized by CuF_6 octahedra elongated along the a and b axis and arranged in an antiferro-distortive pattern in the ab plane.[30] At room temperature, there are two different structural polytypes with antiferro (a-type) and ferrolike (d-type) stacking of the ab planes along the c axis.[40] The JT distortion is associated with the particular orbital order in $KCuF_3$, in which a single hole alternatingly occupies $d_{x^2-z^2}$ and $d_{y^2-z^2}$ orbital states, resulting in a tetragonal compression ($c < a$) of the unit cell. The mechanism responsible for the orbital order in $KCuF_3$ is still being debated in the literature.[6,24,25,41,42,43,44] In particular, purely electronic effects such as in the Kugel-Khomskii theory[24] and the electron-lattice interaction[41] have been discussed as possible driving forces behind the orbital order.

The relatively high (tetragonal) symmetry makes $KCuF_3$ one of the simplest system to study. In particular, in order to describe the JT distortion, only a single internal structure parameter, the shift of the in-plane fluorine atom from the Cu-Cu bond center, is needed. Moreover, $KCuF_3$ has a single hole in the $3d$ shell resulting in absence of multiplet effects. Altogether, the electronic and structural properties of $KCuF_3$ have been intensively studied by density functional theory in the local density approximation (LDA),[2] the generalized gradient approximation (GGA),[3,4] or using the so-called LDA+U approach.[5,6] While the LDA+U calculations account rather well for the value of equilibrium JT distortion in $KCuF_3$,[44] the calculations simultaneously predict long-range antiferromagnetic order which indeed occurs in $KCuF_3$ below T_N ($\sim$ 38 K and 22 K for the a polytype and for the d polytype, respectively).[45] Note, however, that the Néel temperature is much lower than the critical temperature for orbital order which is generally assumed to be as large as the melting temperature ($\sim$ 1000 K). The LDA+U calculations give the correct insulating ground state with the long-range A-type antiferromagnetic and $d_{x^2-z^2}/d_{y^2-z^2}$ antiferro-orbital order,[6,42,44] consistent with the Goodenough-Kanamori-Anderson rules for a superexchange interaction. Non-magnetic LDA calculations instead predict a *metallic* behavior. Moreover, the electronic and structural properties of $KCuF_3$ have been recently reexamined by means of LDA+U molecular-dynamic simulations, indicating a possible symmetry change and challenging the original assignment of tetragonal symmetry.[44] This symmetry change seems to allow for a better understanding of Raman,[46] electronic paramagnetic resonance,[47,48] and

7

x-ray resonant scattering[49] properties at $T \approx T_N$. However, the details of this distortion have not been fully resolved yet.

The LDA+U approach is able to determine electronic properties and the JT distortion in KCuF$_3$ rather well,[44] but the application of this approach is limited to temperatures below T_N. LDA+U cannot explain the properties at $T > T_N$ and, in particular, at room temperature, where KCuF$_3$ is a correlated paramagnetic insulator with a robust JT distortion which persists up to the melting temperature.

Here we present an application of the GGA+DMFT computational scheme formulated in terms of plane-wave pseudopotentials[25,26] which allows us to determine the structural properties, in particular, the amplitude of the equilibrium JT distortion and its energetics, in *paramagnetic* KCuF$_3$. We also report results of a structural optimization, at constant volume (constant external pressure) and lattice symmetry, including optimization of the unit cell shape and fluorine atomic positions.

B. Electronic structure and orbital order

In this section, we present results of the GGA and GGA+DMFT electronic structure calculations of paramagnetic insulator KCuF$_3$. In these calculations we have used the experimental room-temperature crystal structure with space group $I4/mcm$ and lattice constants $a = 5.855$ and $c = 7.852$ Å.[30] The calculations were performed for different values of the JT distortion defined accordingly as $\delta_{\mathrm{JT}} = \frac{1}{2}(d_l - d_s)/(d_l + d_s)$ where d_l and d_s denote the long and short Cu-F bond distances in the ab plane of CuF$_6$ octahedra, respectively, and $2(d_l + d_s) = a$. In the following we express the distortion δ_{JT} in percent of the lattice constant a, e.g., $\delta_{\mathrm{JT}} = 0.002 \equiv 0.2$ %. In our investigation we consider $0.2\% \leq \delta_{\mathrm{JT}} \leq 7\%$. The structural data[30] at room-temperature yield $\delta_{\mathrm{JT}} = 4.4$ %. In the present calculations we keep the lattice parameters a and c and the space group symmetry fixed, whereas the structural optimization involving change of both the JT distortion and lattice constants will be discussed in the following section.

We first calculate the non-magnetic GGA electronic structure of KCuF$_3$, employing the plane-wave pseudopotential approach.[3,50] For these calculations we use the Perdew-Burke-Ernzerhof exchange-correlation functional together with Vanderbilt ultrasoft pseudopotentials for copper and fluorine, and a soft Troullier-Martin pseudopotential for potassium. The

nonlinear core correction to the exchange-correlation potential has been included to account for the overlap between the valence and core electrons. All calculations are carried out in a tetragonal unit cell which contains two formula units (10 atoms) per primitive unit cell. We use a kinetic-energy cutoff of 75 Ry for the plane-wave expansion of the electronic states. The integration in reciprocal space is performed using a [8,8,8] Monkhorst-Pack k-point grid.

For all values of δ_{JT} considered here, the non-magnetic GGA yields a *metallic* rather than the experimentally observed insulating behavior, with an appreciable orbital polarization due to the crystal field splitting. This is shown in Fig. 1 which presents the GGA density of states and the corresponding band structure calculated for $\delta_{\mathrm{JT}} = 4.4$ %. Overall, the non-magnetic GGA results qualitatively agree with previous band-structure calculations.[6,42,44] The Cu t_{2g} states are completely occupied and located at about 1-2 eV below the Fermi level. Partially filled bands at the Fermi level originate from the Cu e_g orbitals. We note that an increase of the JT distortion results in a considerable enhancement of the crystal field splitting between $x^2 - y^2$ and $3z^2 - r^2$ bands (in the local frame[51]) that leads to an appreciable depopulation of the $x^2 - y^2$ orbital. There is a minor narrowing of the t_{2g} and e_g bands of ~ 0.2 and 0.1 eV, respectively, as well as a slight up-shift of the center of gravity of the t_{2g} bands (~ 0.1 eV) with decreasing JT distortion.

In Fig. 2 we display our results for the GGA total energy as a function of the JT distortion δ_{JT}. Notice that, in agreement with previous studies,[6,44] the electron-lattice interaction alone is found insufficient to stabilize the orbitally ordered insulating state. The non-magnetic GGA calculations not only give a metallic solution, but its total energy profile is seen to be almost constant for $\delta_{\mathrm{JT}} < 4$ %, with a very shallow minimum at about 2.5 %. This would imply that KCuF$_3$ has no JT distortion for temperature above 100 K, which is in clear contradiction to experiment. Obviously, a JT distortion by itself, without the inclusion of electronic correlations, cannot explain the experimentally observed orbitally ordered *insulating* state in paramagnetic KCuF$_3$.

To proceed further, we consider the partially filled Cu e_g orbitals as correlated orbitals and construct an effective low-energy Hamiltonian $\hat{H}_{DFT}$ for each value of the JT distortion δ_{JT} considered above. This is achieved by employing the pseudopotential plane-wave GGA results and making a projection onto atomic-centered symmetry-constrained Cu e_g Wannier orbitals.[26] The resulting Cu $x^2 - y^2$ and $3z^2 - r^2$ Wannier orbitals calculated for $\delta_{\mathrm{JT}} = 4.4$ % are shown Fig. 3. Taking the local Coulomb repulsion $U = 7$ eV and Hund's rule exchange
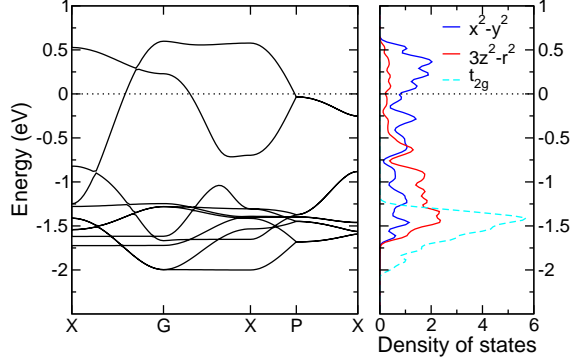
FIG. 1: (color online) Band structure and orbitally resolved Cu t_{2g} and e_g spectral densities of paramagnetic KCuF$_3$ as obtained by non-magnetic GGA for $\delta_{JT} = 4.4\%$. The zero of energy corresponds to the Fermi level.
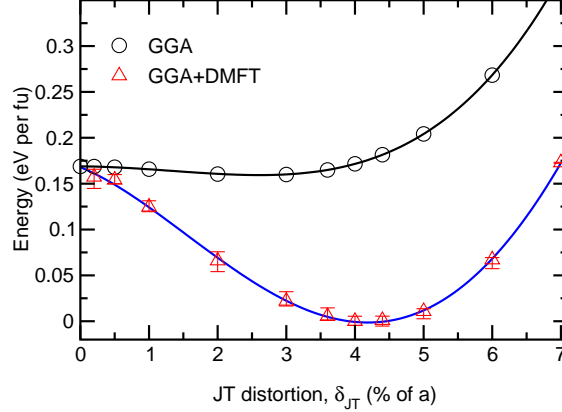

FIG. 2: (color online) Comparison of the total energies of paramagnetic KCuF$_3$ computed by GGA and GGA+DMFT(QMC) as a function of the JT distortion. Error bars indicate the statistical error of the DMFT(QMC) calculations.

$J = 0.9$ eV[6] into account, we obtain the many-body low-energy Hamiltonian (1) for the two ($m = 1, 2$) Cu e_g orbitals, which is further solved (for each value of δ_{JT}) within the single-site DMFT using Hirsch-Fey quantum Monte Carlo (QMC) calculations.[38,52] The calculations have been performed at $T = 1160$ K ($\beta = 10$ eV^{-1}), using 40 imaginary-time slices. The Matsubara sums in Eq. 2 have been taken over $n_{max} = 10^3$ frequencies; this gives accuracy in the total energy calculation better than 10 meV per formula unit.

Using now the expression of Eq. 2, we have calculated the GGA+DMFT total energy for each value of the JT distortion δ_{JT} considered here. The result of the paramagnetic GGA+DMFT computation of the total energy is presented in Fig. 2, where it is compared
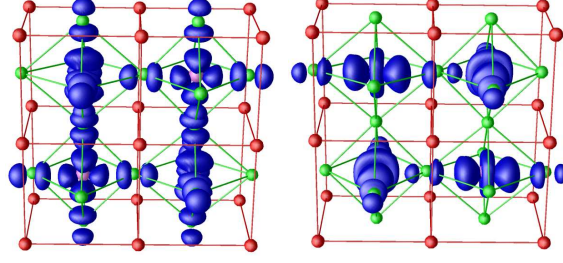
FIG. 3: (color online) $I4/mcm$ primitive cell and Wannier e_g orbitals ($x^2 - y^2$ and $3z^2 - r^2$ in left and right, respectively) as obtained by non-magnetic GGA for $KCuF_3$ with $\delta_{JT} = 4.4$ %. The fluorine atoms and fluorine octahedra are shown in green, the potassium in red, and the Wannier Cu e_g charge density in blue. The local coordinate system is chosen with the z direction defined along the longest Cu-F bond of the CuF_6 octahedron.

with the non-magnetic GGA calculation. In contrast to the GGA result, the inclusion of the electronic correlations among the partially filled Cu e_g states in the GGA+DMFT approach leads to a very substantial lowering of the total energy by ~ 175 meV per formula unit. This implies that the strong JT distortion persists up to the melting temperature (> 1000 K), in agreement with experiment. This finding is in strong contrast to the absence of JT distortion above 100 K predicted by GGA. The minimum of the GGA+DMFT total energy is located at the value $\delta_{JT} \approx 4.2$ %, which is also in excellent agreement with the experimental value of 4.4 %.[30] Note however that the total energy minimum position depends on the value of Coulomb interaction parameter U. Thus, the calculations of the total energy minima for $U = 6$ eV and $U = 8$ eV result in optimal JT distortions of 4.15 % and 4.6 %, respectively. We note that GGA+DMFT calculations correctly describe both electronic and structural properties of paramagnetic $KCuF_3$. This shows that the JT distortion in paramagnetic $KCuF_3$ is caused by electronic correlations.

Figure 4 shows the spectral density of paramagnetic $KCuF_3$, obtained from the QMC data by the maximum entropy method for several values of the JT distortion δ_{JT}. Most importantly, a paramagnetic insulating state with a substantial orbital polarization is obtained for all δ_{JT} considered here. The energy gap is in the range 1.5–3.5 eV, and increases with increasing of δ_{JT}. The sharp feature in the spectral density at about -3 eV corresponds to the fully occupied $3z^2 - r^2$ orbital,[51] whereas the lower and upper Hubbard bands are predominantly of $x^2 - y^2$ character and are located at -5.5 eV and 1.8 eV, respectively. The
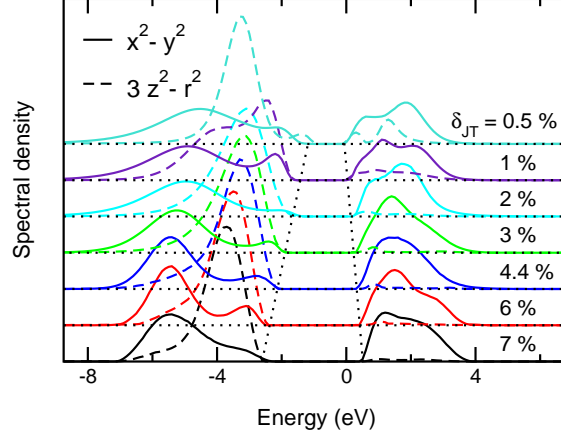
FIG. 4: (color online) Orbitally resolved Cu e_g spectral densities of paramagnetic $KCuF_3$ as obtained by GGA+DMFT(QMC) for different values of the JT distortion. The resulting orbitally resolved spectral density which is shown here by solid [dashed] line is predominantly of $x^2 - y^2$ [$3z^2 - r^2$] character (in the local frame[51]).

corresponding Cu e_g Wannier charge density calculated for the experimental value of JT distortion of 4.4 % is presented in Fig. 5. The GGA+DMFT results clearly show an alternating occupation of the Cu $d_{x^2-z^2}$ and $d_{y^2-z^2}$ hole orbitals, corresponding to the occupation of a $x^2 - y^2$ hole orbital in the local coordinate system,[51] which implies antiferro-orbital order.

The above calculations have been performed for the paramagnetic phase of $KCuF_3$. The Néel temperature ($T_N \sim 22 - 38$ K for different types of orbital order[45]) is much lower than the temperature of present calculations. However, it is known that the ordering temperature might be overestimated by the single-site DMFT approximation, as is common for mean-field theories. To prove the stability of the paramagnetic solution at high temperatures (with respect to the A-type antiferromagnetic one) we have carried out spin-polarized GGA+DMFT calculation at $T = 560$ K. This calculation has been performed for the A-type antiferromagnetic structure using the experimental room-temperature crystal structure of $KCuF_3$ with $\delta_{JT} = 4.4$ %. However, in agreement with experiment, the calculation gives paramagnetic insulating solution with the orbital order as it has been found above.
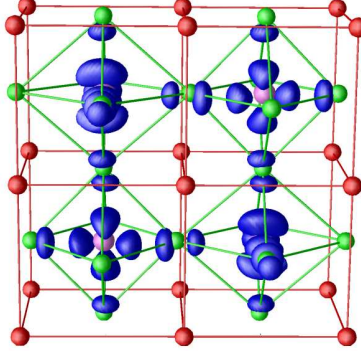
FIG. 5: (color online) $I4/mcm$ primitive cell and hole orbital order as obtained by the GGA+DMFT calculation for paramagnetic $KCuF_3$ with $\delta_{JT} = 4.4$ %. The fluorine atoms and fluorine octahedra are shown in green, the potassium in red, and the Wannier Cu e_g charge density in blue. The local coordinate system is chosen with the z direction defined along the longest Cu-F bond of the CuF_6 octahedron.

C. Optimized structure

To proceed further, we perform a structural optimization of paramagnetic $KCuF_3$. For simplicity, the optimization was performed only for two independent structural parameters, the lattice constant a and the JT distortion δ_{JT}, keeping the space group symmetry (tetragonal $I4/mcm$) and the experimental value of the unit cell volume (taken at the ambient pressure at room temperature) unchanged.[30]

The calculations have been performed in two steps. In the first, we calculate non-magnetic GGA electronic structure for different values of δ_{JT} and lattice constant a. Note that in order to keep the unit cell volume constant, the value of tetragonal distortion (c/a) was changed accordingly. In Figure 6 (a) we plot the total energies obtained by GGA for different JT distortion δ_{JT} as a function of the lattice constant a. The data points were further interpolated by smooth curvies, whereas the result of the total energy variation — the line that connects the minima of the corresponding curves — is marked by black arrows. We note that the result of the GGA structural optimization, the variation of the total energy, is seen to be constant for $\delta_{JT} < 2$ % with the end point at $a \sim 5.75$ Å. This implies the absence of the cooperative JT distortion and results in a nearly cubic ($c/a \approx 1.0$) unit cell, which is in clear contradiction to experiment.[30]

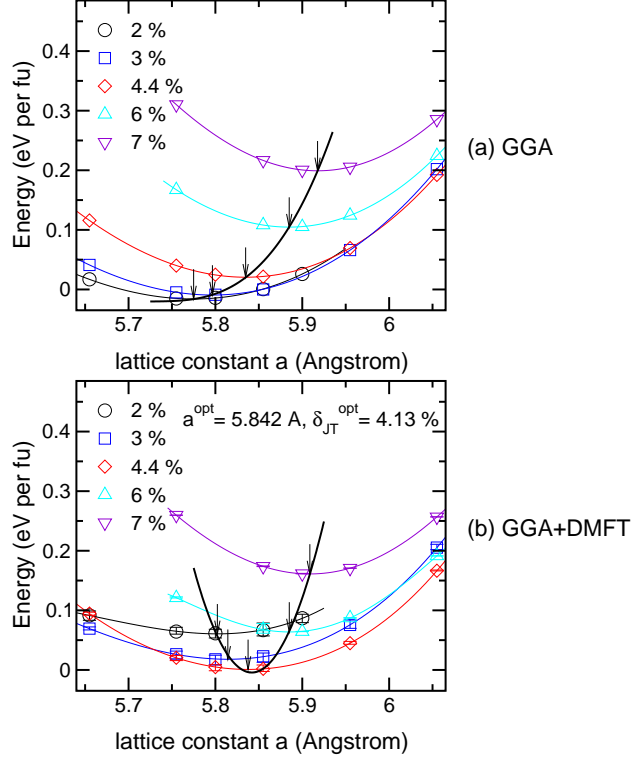In the second step, we construct the effective low-energy Hamiltonian for the partially

FIG. 6: (color online) Comparison of the total energies of paramagnetic $KCuF_3$ computed by GGA (a) and GGA+DMFT(QMC) (b) for different values of the JT distortion δ_{JT} as a function of the lattice constant a. Result of the total energy variation is marked by black arrows. Error bars indicate the statistical error of the DMFT(QMC) calculations.

filled Cu e_g orbitals for each value of the JT distortion δ_{JT} and the lattice constant a considered here, and compute the corresponding total energies using GGA+DMFT approach (see Fig. 6 (b)).[25] In contrast to the structural optimization within GGA, the inclusion of the electronic correlations among the partially filled Cu e_g states in the GGA+DMFT method not only correctly describes the spectral properties, but also leads to a very prominent minimum in the resulting total energy variation. The minimum is located at the value $a = 5.842$ Å and $\delta_{JT} \approx 4.13$ %, which is in excellent agreement with experimental value $a = 5.855$ Å and $\delta_{JT} \approx 4.4$ %. Note that in contrast to GGA, the structural optimization within GGA+DMFT also correctly predicts the tetragonal compression of the unit cell with $c/a \approx 0.95$.[30]

IV. APPLICATION TO LaMnO$_3$

A. Crystal structure and magnetic properties

LaMnO$_3$ is another prototype of a material with a cooperative Jahn-Teller distortion and orbital order. It stands in line with the colossal magnetoresistance manganites whose parent compound it is.[53] At ambient pressure and temperature it has an orthorhombic GdFeO$_3$-like crystal structure with space group $Pnma$ and four formula units (20 atoms) per primitive cell.[31] The Mn ions have octahedral oxygen surrounding and are in a high-spin $3d^4$ electronic configuration due to Hund's rule coupling, with three electrons in the $t_{2g\uparrow}$ orbitals and a single electron in an $e_{g\uparrow}$ orbital ($t_{2g}^3 e_g^1$ orbital configuration). There are two types of structural instabilities which give rise to the changes relative to the cubic perovskite structure. The first is a JT instability due to the orbital degeneracy that lifts the cubic degeneracy at Mn e_g states due to developing the cooperative JT distortion of the MnO$_6$ octahedra. The second is related to a large ion-size misfit parameter $\sqrt{2}(R_O+R_{Mn})/(R_O+R_{La})$ which favors rotations of the octahedra to accommodate a more efficient unit cell space filling. R_{Mn}, R_{La}, and R_O are the ionic radii of Mn, La, and O ions, respectively. The cooperative JT distortion lifts the e_g-orbital degeneracy and leads to an alternating occupation of $d_{3x^2-r^2}$ and $d_{3y^2-r^2}$ electron orbitals in the ab plane (antiferro-orbital ordering) and to a tetragonal compression of the unit cell. The rotations of the octahedra lower the symmetry further, finally leading to the orthorhombic unit cell. In the paramagnetic $Pnma$ phase the JT distortion experimentally persists up to $T_{JT} \approx 750$ K. At this temperature, LaMnO$_3$ undergoes a structural phase transition,[32] with volume collapse[33] to a nearly cubic structure in which orbital order and JT distortion vanish.[32] A quenching of the JT distortion has also been reported in the room-temperature paramagnetic phase under hydrostatic pressure ~ 18 GPa. At ~ 32 GPa it is followed by an insulator-metal transition.[54]

At temperatures $T < T_N \sim 140$ K, which are much lower than $T_{JT} \sim 750$ K where the JT distortion vanishes, LaMnO$_3$ shows A-type long-range antiferromagnetic order consistent with the Goodenough-Kanamori-Anderson rules for a superexchange interaction with $d_{3x^2-r^2}/d_{3y^2-r^2}$ antiferro-orbital order.[31,32] This is also found in spin polarized LDA/GGA and LDA+U calculations using the experimental values of the crystal structure parameters. In this particular case, both magnetic LDA/GGA and LDA+U calculations result in the

qualitatively correct insulating ground state with long-range A-type antiferromagnetic and antiferro-orbital order.[55,56] However, the subsequent structural optimization within the magnetic LDA/GGA calculations results in a *metallic* solution with *reduced* JT distortion.[56,57] In this situation, only the LDA+U scheme is found to give, at equilibrium, the correct insulating character of the low-temperature antiferromagnetic phase and a JT distortion in satisfactory agreement with experiment.[57] Nevertheless, we have to note again that application of this approach is limited to temperatures below T_N. Therefore, LDA+U cannot describe the properties of LaMnO$_3$ at $T > T_N$ and, in particular, at room temperature, where LaMnO$_3$ is a correlated *paramagnetic* insulator with a robust JT distortion. The electronic properties of paramagnetic LaMnO$_3$ have already been studied within the LDA+DMFT approach. In particular, Pruschke and Zölfl[58] studied the electronic and magnetic properties and found an additional increase of the orbital polarization below T_N. Yamasaki *et al.*[59] examined the electronic structure in order to address the origin of the high-pressure metal-insulator transition. Pavarini and Koch[60] investigated the temperature dependence of the orbital polarization to find the origin of the cooperative JT distortion and orbital order. However, no attempt has been made to determine the structural properties and, in particular, the value of the cooperative JT distortion of paramagnetic LaMnO$_3$ so far.

We present here the results of an application of the GGA+DMFT computational scheme formulated in terms of plane-wave pseudopotentials[25,26] to study the electronic and structural properties of paramagnetic LaMnO$_3$. These are the first results of a structural optimization where the stability of the cooperative JT distortion in paramagnetic LaMnO$_3$ was investigated. In principle, this application can be further extended to investigate the structural stability as a function of temperature. Such a full structural optimization will be interesting to study the disappearance of the JT distortion at $T \sim T_{JT}$. However, this is beyond the scope of the present work.

B. Electronic structure and orbital order

In this section, we turn to the results of the GGA and GGA+DMFT electronic structure calculations of paramagnetic LaMnO$_3$. In these calculations, we have used the orthorhombic *Pnma* crystal structure as reported by Elemans *et al.*, with lattice constants $a = 5.742$, $b = 7.668$, and $c = 5.532$ Å.[31] Similar to KCuF$_3$ we change the value of JT distortion δ_{JT},
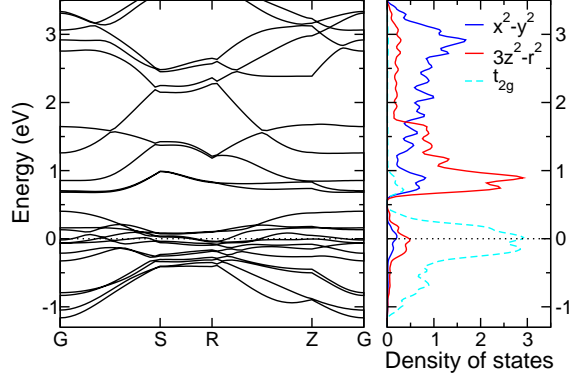
FIG. 7: (color online) Orbitally resolved Mn t_{2g} and e_g spectral densities of paramagnetic LaMnO$_3$ as obtained by non-magnetic GGA for $\delta_{JT} = 0.138$. The zero of energy corresponds to the Fermi level.

which is now defined as the ratio between the difference of the long (d_l) and the short (d_s) bond distances and the mean Mn-O distance in the basal ab plane, i.e., $\delta_{JT} = 2(d_l - d_s)/(d_l + d_s)$. Structural data[31] yield $\delta_{JT} = 0.138$. Note that in the calculation we change only the parameter δ_{JT} ($0 \leq \delta_{JT} \leq 0.2$) and keep the value of the MnO$_6$ octahedron tilting and rotation fixed.

Using the plane-wave pseudopotential calculation scheme, we calculated the non-magnetic GGA electronic structure[3,50] of paramagnetic LaMnO$_3$. We employed the Perdew-Burke-Ernzerhof exchange-correlation functional together with Vanderbilt ultrasoft pseudopotentials, including a nonlinear core correction to the exchange-correlation potential. All calculations were carried out in a 20-atom orthorhombic $Pnma$ unit cell. We used a kinetic-energy cutoff of 45 Ry for the plane-wave expansion of the electronic states. The integration in reciprocal space was performed using a [10,10,10] Monkhorst-Pack k-point grid.

For all values of δ_{JT} considered here the non-magnetic GGA calculations give a metallic solution with a considerable orbital polarization due to the crystal field splitting. Overall, these results qualitatively agree with previous band structure calculations,[61] namely, that the GGA cannot describe a paramagnetic insulating behavior which is found in experiment. We notice that even for the large δ_{JT} value of 0.2 ($\sim$ 45 % larger than found in experiment[31]) the GGA calculations predict a metal. The non-magnetic GGA density of states and the corresponding band structure calculated for the JT distortion $\delta_{JT} = 0.138$ are presented in Fig. 7. In contrast to KCuF$_3$, the partially filled bands at the Fermi level now originate
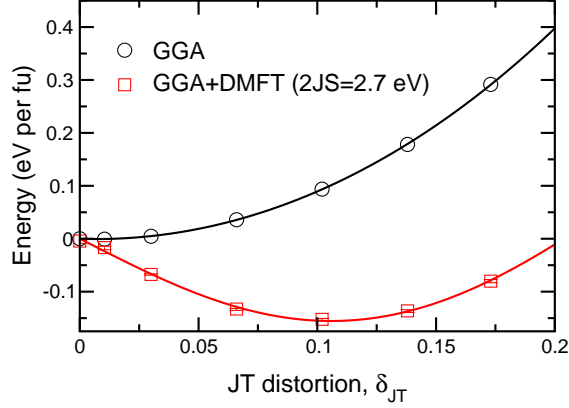
FIG. 8: (color online) Comparison of the total energies of paramagnetic LaMnO$_3$ computed by GGA and GGA+DMFT(QMC) as a function of the JT distortion. Error bars indicate the statistical error of the DMFT(QMC) calculations.

from the Mn t_{2g} orbitals. This is due to the $3d^4$ electronic configuration of Mn ions and the fictitious paramagnetic state without local moments obtained by non-magnetic GGA. In fact, the Hund's rule coupling results in a strong on-site spin polarization of the Mn t_{2g} and e_g orbitals. Therefore, the $t_{2g\uparrow}$ states become completely occupied and located below the Fermi level, while the remaining electron fills the $e_{g\uparrow}$ states. An increase of the JT distortion results in considerable enhancement of the crystal field splitting between $x^2 - y^2$ and $3z^2 - r^2$ bands (in the local frame[62]) which reaches ~ 1.1 eV for $\delta_{JT} = 0.138$. The overall e_g band width is about 2.8-3.0 eV, which is remarkably much smaller than the estimates of the Coulomb interaction parameter U found in the literature.[59,61]

In Fig. 8 we display our results for the GGA total energy as a function of the JT distortion δ_{JT}. In contrast to experiment, the non-magnetic GGA calculations give a metallic solution without cooperative JT distortion. Thus, the GGA total energy is almost parabolic which implies the absence of a cooperative JT distortion and is in clear contradiction to experiment.[31,32] As in the case of KCuF$_3$ this shows the importance of electronic correlations, without which the experimentally observed orbitally ordered, insulating state in paramagnetic LaMnO$_3$ cannot be explained.

Next, we turn to the GGA+DMFT results where we treat the Mn e_g orbitals as correlated orbitals. Using pseudopotential plane-wave approach, we perform a projection onto atomic-centered symmetry-constrained Mn e_g Wannier orbitals,[26] which are shown in Fig. 9. In this calculation we assume that three (among the $3d^4$ electronic configuration) electrons are
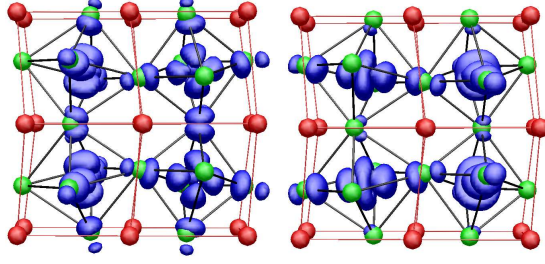
FIG. 9: (color online) *Pnma* primitive cell and the Wannier e_g orbitals ($x^2 - y^2$ and $3z^2 - r^2$ in left and right, respectively[62]) for LaMnO$_3$ with $\delta_{\text{JT}} = 0.138$ according to the non-magnetic GGA calculation. The oxygen atoms and oxygen octahedra are shown in green, the lanthanum in red, and the Wannier Mn e_g charge density in blue.

localized in the t_{2g} orbitals. Therefore, they are treated as classical spins S, with a random orientation above T_N (i.e., there is no correlation between different Mn sites), which couple to the e_g electron with an energy JS. This coupling can be estimated as the energy of the splitting of the $e_{g\uparrow}$ and $e_{g\downarrow}$ bands in the ferromagnetic band-structure calculations and gives an additional term in the Hamiltonian (1), namely,

$$
\hat{H} = \hat{H}_{DFT} + U \sum_{im} \hat{n}_{im\uparrow}\hat{n}_{im\downarrow} - JS \sum_{im}(\hat{n}_{im\uparrow} - \hat{n}_{im\downarrow})
$$
$$
+ \sum_{im \neq m'\sigma\sigma'}(V - \delta_{\sigma\sigma'}J)\hat{n}_{im\sigma}\hat{n}_{im'\sigma'} - \hat{H}_{DC}. \tag{5}
$$

This corresponds to the ferromagnetic Kondo-lattice model (KLM) Hamiltonian with an on-site Coulomb repulsion between e_g electrons, which has been intensively studied as a possible microscopic model to explain colossal magnetoresistance in manganites.[34,35] We note that in order to calculate the total energy one needs to modify Eq. 2 by adding the expectation value of the JS term which describes the total energy gain due to the spin polarization of the e_g orbitals at the Mn site.

We take the local Coulomb repulsion $U = 5$ eV, the Hund's rule exchange $J = 0.75$ eV, and $2JS = 2.7$ eV from the literature[59] and further solve the many-body Hamiltonian (5) for each value of δ_{JT} using the single-site DMFT with Hirsch-Fey quantum Monte Carlo (QMC) calculations.[38,52] The calculations were again performed at $T = 1160$ K ($\beta = 10$ eV^{-1}), using 40 imaginary-time slices.

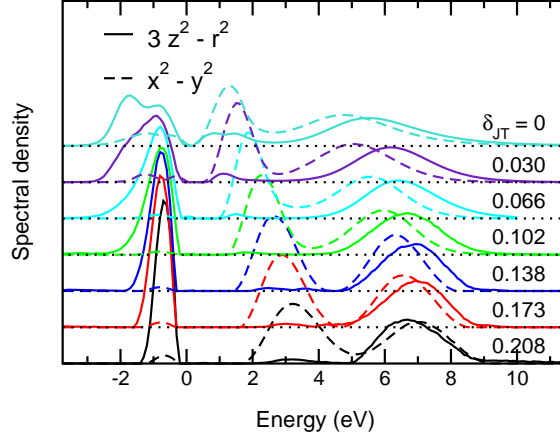In Fig. 8 we present the result of the paramagnetic GGA+DMFT computation of the

FIG. 10: (color online) Orbitally resolved Mn e_g spectral densities of paramagnetic LaMnO$_3$ as obtained by GGA+DMFT(QMC) for different values of the JT distortion. The resulting orbitally resolved spectral density shown by solid [dashed] line is predominantly of $3z^2-r^2$ $[x^2-y^2]$ character (in the local frame[62]).

total energy, where it is compared with the results of the non-magnetic GGA calculation. In contrast to the GGA result, the correlated electron problem solved by GGA+DMFT approach gives a substantial total energy gain of $\sim$ 150 meV per formula unit. This implies that the cooperative JT distortion indeed persists up to high temperatures ($T > 1000$ K), while in GGA a JT distortion does not occur at all. Taking into account that the calculations have been performed for the low-temperature crystal structure of LaMnO$_3$[31] this estimate (150 meV) is in good agreement with $T_{JT} \sim 750$ K at which the JT distortion vanishes.[32,33] However, the structural change as a function of temperature in LaMnO$_3$, as well as the disappearance of the orbital-order and JT distortion[32,33] remains an open problem. The minimum of the GGA+DMFT total energy is located at the value $\delta_{\rm JT} \sim 0.11$, which is also in good agreement with the experimental value of 0.138.[31,32] We note that GGA+DMFT calculations correctly describe both electronic and structural properties of paramagnetic LaMnO$_3$. This shows that the JT distortion in paramagnetic LaMnO$_3$ is caused by electronic correlations.

The spectral densities of paramagnetic LaMnO$_3$ calculated for several values of the JT distortion $\delta_{\rm JT}$ using the maximum entropy analysis of the QMC data are shown in Fig. 10. For large $\delta_{\rm JT}$, we find a strong orbital polarization which gradually decreases for decreasing JT distortion. The occupied part of the e_g density is located at about -2 – -1 eV and corre-
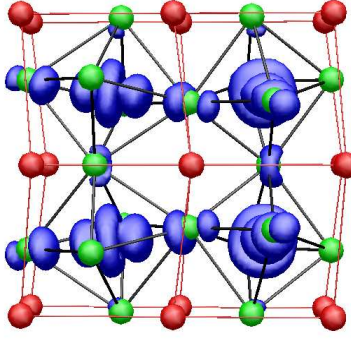
FIG. 11: (color online) *Pnma* primitive cell and orbital order as obtained by the GGA+DMFT calculation for paramagnetic LaMnO$_3$ with $\delta_{JT} = 0.138$. The oxygen atoms and oxygen octahedra are shown in green, the lanthanum in red, and the Wannier Mn e_g charge density in blue.

sponds to the e_g states with spin parallel to the t_{2g} spin at that site. It has predominantly Mn $d_{3x^2-r^2}$ and $d_{3y^2-r^2}$ orbital character with a considerable admixture of $d_{z^2-r^2}$ for small JT distortions. The energy gap is about 2 eV for large δ_{JT} and considerably decreases with decreasing δ_{JT}, resulting in a pseudogap behavior at the Fermi level for $\delta_{JT} = 0$. In Fig. 11 we show the corresponding Mn e_g Wannier charge density computed for the experimental JT distortion value of $\delta_{JT} = 0.138$. The result clearly show an alternating occupation of the Mn $d_{3x^2-r^2}$ and $d_{3y^2-r^2}$ orbitals, corresponding to the occupation of a $3z^2 - r^2$ orbital in the local frame,[62] which implies antiferro-orbital order. Thus, in agreement with experiment, the calculations give a paramagnetic insulating solution with antiferro-orbital order and stable JT distortion.

V. SUMMARY AND CONCLUSIONS

In conclusion, by formulating GGA+DMFT — the combination of the *ab initio* band structure calculation technique GGA with the dynamical mean-field theory — in terms of plane-wave pseudopotentials,[25,26] we constructed a robust computational scheme for the investigation of complex materials with strong electronic interactions. Most importantly, the computational scheme presented here allows us to explain correlation-induced structural transformations, shifts of equilibrium atomic positions and changes in the lattice structure, and to perform a structural optimization of *paramagnetic* solids. We presented applica-

tions of this approach to two prototypical Jahn-Teller materials, $KCuF_3$ and $LaMnO_3$, and computed the orbital order and cooperative JT distortion in these compounds. In particular, our results obtained for the paramagnetic phase of $KCuF_3$ and $LaMnO_3$, namely an equilibrium Jahn-Teller distortion δ_{JT} of 4.2 % and 0.11, respectively, and antiferro-orbital order, agree well with experiment. The present approach overcomes the limitations of the LDA+U method and is able to determine correlation-induced structural transformations in both paramagnetic and long-range magnetically ordered solids, and can thus be employed for the lattice optimization and molecular-dynamic simulations of these systems. The GGA+DMFT scheme presented in this paper opens the way for fully microscopic investigations of the structural properties of strongly correlated electron materials such as lattice instabilities observed at correlation-induced metal-insulator transitions.

---

[1] M. Imada, A. Fujimori, and Y. Tokura, Rev. Mod. Phys. **70**, 1039 (1998); Y. Tokura and N. Nagaosa, Science **288**, 462 (2000); E. Dagotto, Science **309**, 257 (2005).

[2] R. O. Jones and O. Gunnarsson, Rev. Mod. Phys. **61**, 689 (1989).

[3] J. P. Perdew, K. Burke, and M. Ernzerhof, Phys. Rev. Lett. **77**, 3865 (1996).

[4] In general, GGA tends to give better results than LDA for the electronic and structural properties of complex oxides and related materials. See, D. R. Hamann, Phys. Rev. Lett. **76**, 660 (1996) and H. Sawada, Y. Morikawa, K. Terakura, and N. Hamada, Phys. Rev. B **56**, 12154 (1997).

[5] V. I. Anisimov, J. Zaanen, and O. K. Andersen, Phys. Rev. B **44**, 943 (1991); V. I. Anisimov,

F. Aryasetiawan, and A. I. Lichtenstein, J. Phys.: Condens. Matter **9**, 767 (1997).

6 A. I. Liechtenstein, V. I. Anisimov, and J. Zaanen, Phys. Rev. B **52**, R5467 (1995).

7 H. J. Jansen and A. J. Freeman, Phys. Rev. B **30**, 561 (1984).

8 S. Baroni, S. de Gironcoli, A. Dal Corso, and P. Giannozzi, Rev. Mod. Phys. **73**, 515 (2001); P. Giannozzi, S. Baroni, N. Bonini, M. Calandra, R. Car, C. Cavazzoni, D. Ceresoli, G. L. Chiarotti, M. Cococcioni, I. Dabo, A. Dal Corso, S. Fabris, G. Fratesi, S. de Gironcoli, R. Gebauer, U. Gerstmann, C. Gougoussis, A. Kokalj, M. Lazzeri, L. Martin-Samos, N. Marzari, F. Mauri, R. Mazzarello, S. Paolini, A. Pasquarello, L. Paulatto, C. Sbraccia, S. Scandolo, G. Sclauzero, A. P. Seitsonen, A. Smogunov, P. Umari, and R. M. Wentzcovitch, J. Phys. Condens. Matter **21**, 395502 (2009).

9 P. Blaha, K. Schwarz, G. Madsen, D. Kvasnicka, and J. Luitz, WIEN2k, *An Augmented Plane Wave + Local Orbitals Program for Calculating Crystal Properties* (Karlheinz Schwarz, Techn. Universität Wien, Austria), 2001.

10 G. Kresse and J. Hafner, Phys. Rev. B **47**, 558 (1993); G. Kresse and J. Hafner, Phys. Rev. B **49**, 14251 (1994); G. Kresse and J. Furthmüller, Phys. Rev. B **54**, 11169 (1996).

11 X. Gonze, J.-M. Beuken, R. Caracas, F. Detraux, M. Fuchs, G.-M. Rignanese, L. Sindic, M. Verstraete, G. Zerah, F. Jollet, M. Torrent, A. Roy, M. Mikami, Ph. Ghosez, J.-Y. Raty, and D.C. Allan, Computational Materials Science **25**, 478-492 (2002).

12 M. Soler, E. Artacho, J. D. Gale, A. García, J. Junquera, P. Ordejón, and D. Sánchez-Portal, J. Phys.: Condens. Matter **14**, 2745 (2002).

13 W. Metzner and D. Vollhardt, Phys. Rev. Lett. **62**, 324 (1989); A. Georges, G. Kotliar, W. Krauth, and M. J. Rozenberg, Rev. Mod. Phys. **68**, 13 (1996); G. Kotliar and D. Vollhardt, Phys. Today **57**, No. 3, 53 (2004); G. Kotliar, S. Y. Savrasov, K. Haule, V. S. Oudovenko, O. Parcollet, and C. A. Marianetti, Rev. Mod. Phys. **78**, 865 (2006).

14 V. I. Anisimov, A. I. Poteryaev, M. A. Korotin, A. O. Anokhin and G. Kotliar, J. Phys. Condens. Matt. **9**, 7359 (1997); A. I. Lichtenstein and M. I. Katsnelson, Phys. Rev. B **57**, 6884 (1998); K. Held, I. A. Nekrasov, G. Keller, V. Eyert, N. Blümer, A. K. McMahan, R. T. Scalettar, Th. Pruschke, V. I. Anisimov, and D. Vollhardt, Psi-k Newsletter **56**, 65 (2003); K. Held, I. A. Nekrasov, G. Keller, V. Eyert, N. Blümer, A. K. McMahan, R. T. Scalettar, Th. Pruschke, V. I. Anisimov, and D. Vollhardt, Phys. Status Solidi B **243**, 2599 (2006).

15 K. Held, G. Keller, V. Eyert, D. Vollhardt, and V. I. Anisimov, Phys. Rev. Lett. **86**, 5345 (2001);

E. Pavarini, S. Biermann, A. Poteryaev, A. I. Lichtenstein, A. Georges, and O. K. Andersen, Phys. Rev. Lett. **92**, 176403 (2004); A. I. Poteryaev, A. I. Lichtenstein, and G. Kotliar, Phys. Rev. Lett. **93**, 086401 (2004); S. Biermann, A. Poteryaev, A. I. Lichtenstein, and A. Georges, Phys. Rev. Lett. **94**, 026404 (2005); L. Chioncel, Ph. Mavropoulos, M. Lezaić, S. Blügel, E. Arrigoni, M. I. Katsnelson, and A. I. Lichtenstein, Phys. Rev. Lett. **96**, 197203 (2006); J. Kunes, V. I. Anisimov, S. L. Skornyakov, A. V. Lukoyanov, and D. Vollhardt, Phys. Rev. Lett. **99**, 156404 (2007).

[16] M. I. Katsnelson and A. I. Lichtenstein Phys. Rev. B **61**, 8906 (2000); A. I. Lichtenstein, M. I. Katsnelson, and G. Kotliar, Phys. Rev. Lett. **87**, 067205 (2001); J. Braun, J. Minár, H. Ebert, M. I. Katsnelson, and A. I. Lichtenstein, Phys. Rev. Lett. **97**, 227601 (2006); A. Grechnev, I. Di Marco, M. I. Katsnelson, A. I. Lichtenstein, J. Wills, and O. Eriksson, Phys. Rev. B **76**, 035107 (2007); S. Chadov, J. Minár, M. I. Katsnelson, H. Ebert, D. Ködderitzsch, and A. I. Lichtenstein, Europhys. Lett. **82**, 37001 (2008).

[17] O. K. Andersen, Phys. Rev. B **12**, 3060 (1975); O. K. Andersen and T. Saha-Dasgupta, Phys. Rev. B **62**, R16219 (2000).

[18] K. Held, A. K. McMahan, and R. T. Scalettar, Phys. Rev. Lett. **87**, 276404 (2001); A. K. McMahan, K. Held, and R. T. Scalettar, Phys. Rev. B **67**, 075108 (2003).

[19] B. Amadon, S. Biermann, A. Georges, and F. Aryasetiawan, Phys. Rev. Lett. **96**, 066402 (2006); L. V. Pourovskii, B. Amadon, S. Biermann, and A. Georges, Phys. Rev. B **76**, 235101 (2007).

[20] S. Y. Savrasov, G. Kotliar, and E. Abrahams, Nature (London) **410**, 793 (2001); X. Dai, S. Y. Savrasov, G. Kotliar, A. Migliori, H. Ledbetter, and E. Abrahams, Science **300**, 953 (2003); S. Y. Savrasov and G. Kotliar, Phys. Rev. B **69**, 245101 (2004).

[21] J. Kunes, A. V. Lukoyanov, V. I. Anisimov, R. T. Scalettar, and W. E. Pickett, Nature Materials 7, 198 (2008).

[22] The problem of equilibrium volume of number of simple elements has been also recently addressed by I. Di Marco, J. Minár, S. Chadov, M. I. Katsnelson, H. Ebert, and A. I. Lichtenstein [Phys. Rev. B **79**, 115111 (2009)] and A. Kutepov, S. Y. Savrasov, and G. Kotliar [Phys. Rev. B **80**, 041103 (R) (2009)].

[23] H. A. Jahn and E. Teller, Proc. R. Soc. London Ser. A **161**, 220 (1937).

[24] D. I. Khomskii and K. I. Kugel, Solid State Comm. **13**, 763 (1973); K. I. Kugel and D. I. Khomskii, Sov. Phys. Solid State **17**, 285 (1975); K. I. Kugel and D. I. Khomskii, Sov. Phys.

JETP **52**, 501 (1981); K. I. Kugel and D. I. Khomskii, Sov. Phys. Usp. **25**(4), 231 (1982).

[25] I. Leonov, N. Binggeli, Dm. Korotin, V. I. Anisimov, N. Stojić, and D. Vollhardt, Phys. Rev. Lett. **101**, 096405 (2008).

[26] G. Trimarchi, I. Leonov, N. Binggeli, Dm. Korotin, and V. I. Anisimov, J. Phys.: Condens. Matter **20**, 135227 (2008).

[27] Dm. Korotin, A. V. Kozhevnikov, S. L. Skornyakov, I. Leonov, N. Binggeli, V. I. Anisimov, and G. Trimarchi, The European Physical Journal B **65**, 91 (2008).

[28] B. Amadon, F. Lechermann, A. Georges, F. Jollet, T. O. Wehling, and A. I. Lichtenstein, Phys. Rev. B **77**, 205112 (2008).

[29] For a formulation of LDA+DMFT within a mixed-basis pseudopotential approach see F. Lechermann, A. Georges, A. Poteryaev, S. Biermann, M. Posternak, A. Yamasaki, and O. K. Andersen, Phys. Rev. B **74**, 125120 (2006).

[30] R. H. Buttner, E. N. Maslen, and N. Spadaccini, Acta Cryst. B **46**, 131 (1990).

[31] J. B. A. A. Elemans and B. van Laar, K. R. van der Veen, and B. O. Loopstra, J. Phys. Chem. Solids **3**, 238 (1971).

[32] J. Rodriguez-Carvajal, M. Hennion, F. Moussa, A. H. Moudden, L. Pinsard, and A. Revcolevschi, Phys. Rev. B. **57**, R3189 (1998).

[33] T. Chatterji, F. Fauth, B. Ouladdiaf, P. Mandal, and B. Ghosh, Phys. Rev. B **68**, 052406 (2003).

[34] A. J. Millis, B. I. Shraiman, and R. Mueller, Phys. Rev. Lett. **77**, 175 (1996).

[35] K. Held and D. Vollhardt, Phys. Rev. Lett. **84**, 5168 (2000).

[36] V. I. Anisimov, D. E. Kondakov, A. V. Kozhevnikov, I. A. Nekrasov, Z. V. Pchelkina, J. W. Allen, S.-K. Mo, H.-D. Kim, P. Metcalf, S. Suga, A. Sekiyama, G. Keller, I. Leonov, X. Ren, and D. Vollhardt, Phys. Rev. B **71**, 125119 (2005).

[37] N. Marzari and D. Vanderbilt, Phys. Rev. B **56**, 12847 (1997).

[38] J. E. Hirsch and R. M. Fye, Phys. Rev. Lett **56**, 2521 (1986).

[39] S. Kadota, I. Yamada, S. Yoneyama, and K. Hirakawa, J. Phys. Soc. Jpn. 23, 751 (1967).

[40] A. Okazaki, J. Phys. Soc. Jpn. **26**, 870 (1969); A. Okazaki, J. Phys. Soc. Jpn. **27**, 518B (1969).

[41] J. B. Goodenough, *Magnetism and the Chemical Bond* (Interscience, New York, 1963).

[42] J. E. Medvedeva, M. A. Korotin, V. I. Anisimov, and A. J. Freeman, Phys. Rev. B **65**, 172413 (2002).

[43] E. Pavarini, E. Koch, and A. I. Lichtenstein, Phys. Rev. Lett. **101**, 266405 (2008).

[44] N. Binggeli and M. Altarelli, Phys. Rev. B **70**, 085117 (2004).

[45] M. T. Hutchings, E. J. Samuelsen, G. Shirane, and K. Hirakawa, Phys. Rev. **188**, 919 (1969).

[46] T. Ueda, K. Sugawara, T. Kondo, and I. Yamada, Solid State Commun. **80**, 801 (1991).

[47] I. Yamada, H. Fujii, and M. Hidaka, J. Phys. Condens. Matter **1**, 3397 (1989).

[48] M. V. Eremin, D. V. Zakharov, H.-A. Krug von Nidda, R. M. Eremina, A. Shuvaev, A. Pimenov, P. Ghigna, J. Deisenhofer, and A. Loidl, Phys. Rev. Lett. **101**, 147601 (2008); J. Deisenhofer, I. Leonov, M. V. Eremin, Ch. Kant, P. Ghigna, F. Mayr, V. V. Iglamov, V. I. Anisimov, and D. van der Marel, *ibid.* **101**, 157406 (2008).

[49] L. Paolasini, R. Caciuffo, A. Sollier, P. Ghigna, and M. Altarelli, Phys. Rev. Lett. **88**, 106403 (2002); R. Caciuffo, L. Paolasini, A. Sollier, P. Ghigna, E. Pavarini, J. van den Brink, and M. Altarelli, Phys. Rev. B **65**, 174425 (2002).

[50] Calculations have been performed using the Quantum ESPRESSO package, see Ref. 8, URL http://www.quantum-espresso.org.

[51] The local coordinate system is chosen with the z direction defined along the longest (in ab plane) Cu-F bond of the CuF_6 octahedron.

[52] To simplify the computation we neglected the orbital off-diagonal elements of the local Green's function by applying an additional transformation into the local basis set with a diagonal density matrix during each DMFT iteration.

[53] For a review, see, for example, Y. Tokura, Ed., *Colossal Magnetoresistive Oxides* (Gordon and Breach Science, New York, 2000), and references therein.

[54] I. Loa, P. Adler, A. Grzechnik, K. Syassen, U. Schwarz, M.. Hanfland, G. Kh. Rozenberg, P. Gorodetsky, and M. P. Pasternak, Phys. Rev. Lett. **87**, 125501 (2001).

[55] P. Ravindran, A. Kjekshus, H. Fjellvag, A. Delin, and O. Eriksson, Phys. Rev. B **65**, 064445 (2002); and references therein.

[56] H. Sawada, Y. Morikawa, K. Terakura, and N. Hamada, Phys. Rev. B **56**, 12154 (1997).

[57] G. Trimarchi and N. Binggeli, Phys. Rev. B **71**, 035101 (2005).

[58] Th. Pruschke and M.B. Zölfl, *Advances in Solid State Physics* **40**, 251 (2000); See also R. Peters and Th. Pruschke, cond-mat/0908.3990, where the authors discuss the interplay of orbital and spin degrees of freedom in the two orbital Hubbard model near quarter filling.

[59] A. Yamasaki, M. Feldbacher, Y.-F. Yang, O. K. Andersen, and K. Held, Phys. Rev. Lett. **96**,

166401 (2006); K. Held, O. K. Andersen, M. Feldbacher, A. Yamasaki, and Y.-F. Yang, J. Phys.: Condens. Matter **20**, 064202 (2008).

[60] E. Pavarini and E. Koch, cond-mat/0904.4603.

[61] W.-G. Yin, D. Volja, and W. Ku, Phys. Rev. Lett. **96**, 116405 (2006).

[62] The local coordinate system is chosen such that the GGA Mn $3d$ density matrix has a diagonal form.